Role of the third metal oxide in In-Ga-Zn-O_4 amorphous oxide semiconductors: Alternatives to gallium

Zhaofu Zhang[1], Yuzheng Guo[2], John Robertson[1, *]

[1] Department of Engineering, University of Cambridge, Cambridge, CB2 1PZ, UK
[2] College of Engineering, Swansea University, Swansea, SA1 8EN, United Kingdom
* Email: jr@eng.cam.ac.uk

Abstract: We study the role of the third metal oxide in In-Ga-Zn type oxides (IGZO), Ga_2O_3, by comparing the calculated electronic properties of various alternatives (Al, Y, Hf, Ti, Si, W) to Ga. It is found that Ga_2O_3 causes little disorder in the conduction band minimum (CBM) energy based on In or Zn oxides, and it has a large O vacancy suppression effect, which benefits both a high mobility and a low OFF-current of IGZO. However, other alternative choices give a pronounced conduction band disorder potential due to their higher CBM energies, and thus are not ideal components in amorphous oxide semiconductors. Si and W may reduce the negative bias illumination stress instability by lowering hydrogen induced states to below the bulk valence band maximum but Si is not beneficial for mobility. Their role in back-end-of-line transistors is also noted.

I. Introduction

Amorphous oxide semiconductors (AOS) such as In-Ga-Zn oxide (IGZO) are rapidly displacing hydrogenated amorphous silicon (a-Si:H) as the dominant semiconductor for display applications, benefitting from their much higher electron mobility of over 10 $cm^2/V{\cdot}s$ and their ease of large-area deposition by sputtering [1-3]. Hosono et al [1-3] have noted that post-transition metal ions with a valence structure of $d^{10}s^0$ would produce amorphous oxides whose conduction properties are very insensitive to disorder and give a high electron mobility [1-7]. However, overall, these oxides should also have other properties, such as a low current in the off-state, and also have a good electro-optical stability [8-14]. It is found that the best performance occurs not for a single oxide but a combination of two or three oxides where each component contributes a specific role.

The roles of each oxide are different in IGZO. Of the three oxides, ZnO is a low-cost oxide which has a high mobility semiconductor in its crystalline (c-) phase. Zn in ZnO has the $d^{10}s^0$ electronic structure so that it also retains its high mobility in the amorphous (a-) phase. However ZnO is not easily made amorphous, with amorphisation of ZnO costing 0.4 eV per formula unit [15]. A second conductive oxide should be added to the ZnO to reduce the amorphization energy to be less than 0.15 eV/atom by the mixed alkali effect [15]. An amorphous structure is essential for large area devices in order to be deposited as smooth thin films without grain boundaries and with minimum surface roughness. In_2O_3 has the highest performance as a second conductive oxide because its 5s valence orbital has the largest size [7], which contributes to a high carrier mobility in both its crystalline and amorphous states. Indium was shown by Nomura et al [6] to be a critical ingredient of the oxide. However, In is relatively rare and costly compared to other similar metals and many efforts are made to replace

it. In general there has been great interest to substitute In with a more widely available metal oxide than In.

The role of the third metal oxide in IGZO, Ga_2O_3, has been less discussed. It has been considered to contribute several properties, and various metal oxides such as HfO_2 have been investigated experimentally as alternatives to Ga_2O_3 [16-23]. The first role is that Ga bonds more strongly to oxygen than Zn or In does, so that it acts to increase the formation energy of oxygen vacancies and so suppresses the creation of these vacancies and their associated free carriers [18-20]. A second factor to consider is its effect on the overall effective mass of the conduction band minimum in any ternary oxide, IXZO [19], (X indicates the third metal). Another role of the third oxide could be to minimise any transistor instabilities, either electrical or light-induced [8-14]. Here we consider this question by analyzing the calculated electronic properties of the various third oxide alternatives in IGZO, namely IXZO (X=Ga, Al, Y, Hf, Ti, Si), both in the c- phase and in the a- phase.

There have been other applications besides displays and other ternary combinations are of interest. Recently, the amorphous oxides have been particularly interesting for back-end-of-line embedded memory devices, where the ultra-low OFF current has been of interest for dynamic random-access memory (DRAM) selector switches and related uses. Methods to lower the density of gap states and ways to vary the Schottky barrier height and its effect on parasitic resistance have been of interest [24-27]. In this case variation of the barrier height may be required.

II. Methods

The calculations used the CASTEP density-functional plane-wave codes [28]. All calculations were converged to a residual energy difference of 10^{-5} eV and a residual force tolerance of 0.02 eV/Å on each atom. We use the norm-conserving pseudopotentials with a plane wave cut-off energy of 680 eV, and the pseudopotential for oxygen was generated by the OPIUM method [29]. A 3×3×3 k-point mesh was adopted.

The continuous random networks of a-IXZO were generated by using ab-initio molecular dynamics (AIMD) on a supercell of 14 $InXZnO_4$ units. The AIMD calculations anneal the networks at 2000 K for 5 ps, then quench them to 300 K with the rate of 10 K/ps, followed by further relaxation and electronic analysis. The mass density of a-IGZO is 6.07 g/cm^3. It should be addressed that the generalized gradient approximation (GGA) exchange-correlation functional grossly underestimates the band gap of ZnO and similar post-transition metal oxides [30], while it is necessary to maintain the large band gap during the MD amorphization process to avoid any side effects. So the GGA+U treatment [30-32] was used in MD to partly correct the band gap, without excessive computational cost, similar to our previous work [15,33]. It is known that the GGA functional gives ZnO a severely underestimated band gap of only ~0.8 eV, while GGA+U with U=~5 eV on Zn-d gives a band gap of only ~1.5 eV [30], still far below the experimental gap. Thus, the on-site potential of U = 5 eV on both the transition metal d orbital and on the O-p orbital was used in this work, which gives a gap of 2.34 eV for the final a-IGZO. It is not recommended to use an unphysically large U value for Zn-d, while a

combination of the on-site U potentials gives a more reasonable band structure [15], and is enough to satisfy the basic need to maintain a large gap in the MD process. Other U values can also be used for this goal.

The crystalline structures of c-IXZO were calculated for ternary oxides in the A_2BO_4 spinel structure, where A is a trivalent metal (In, Ga) and B is a divalent metal (Zn), as is shown in Fig. 1. We did not use the crystalline IGZO structure whose unit cell is long and thin [15] and the spinel structure avoids creating several O sites that have no Ga-site neighbor in the crystalline IGZO structure. Other trivalent alternatives to Ga like Al and Y can also be treated in the spinel structure in the same way. We can also accommodate 4-valent metals (Hf, Ti and Si) in a spinel lattice by lowering the content of the divalent species, such as in the $In_2Hf_2ZnO_8$ stoichiometry.

After MD and final relaxation, the electronic spectra were analysed by the more expensive Heyd-Scuseria-Ernerzhof (HSE) hybrid functionals [34], which mixes in a fraction of non-local Hartree-Fock (HF) exchange into GGA and thus more accurately corrects the band gap error than the GGA+U method. Oba et al [35] reported that an HF fraction of α=0.375 can fit the ZnO band gap to the experimental value. In this work, we use α=0.35 in HSE, and this reproduces the experimental gap of 3.13 eV for a-IGZO.

III. Results and discussion

A key point is that IGZO is to be used as a transistor channel, not as a transparent conductor. Thus it is critical that the current can be switched on and off by a small forward bias. The ability of the third oxide to increase the cost of oxygen vacancy donors and minimise free carrier creation is an important feature in IGZO. The energy cost of an oxygen vacancy in a binary oxide MO is close to the formation energy per oxygen of the bulk binary oxide [36]. This formation energy is plotted against the metal's work function [37] for various oxides of interest in Fig. 2(a). Here it is seen that the formation energy per O atom of metal oxides increases roughly linearly with decreasing metal work function before saturating for metals more electropositive than Hf. Furthermore, Fig. 2(a) shows that ZnO and In_2O_3 have moderate heats of formation of about -3.1 eV per O atom. The more electropositive metals with oxides of higher formation energy (i.e., more negative values) than ZnO and In_2O_3 would increase the cost of the oxygen vacancy. The highly electropositive metals particularly early-transition metals like Hf, Y or La or main group metals like Al, have the oxides with the highest heats of formation. Thus, these alternatives would have a better O vacancy suppression effect than Ga.

The overall formation energy of an oxygen vacancy varies with the oxide composition and its atomic structure. This is seen in Fig. 2(b), which shows the weighted average cost of an oxygen vacancy in the spinel-like crystalline structure. The vacancy formation energies are discussed at a constant value, the O-poor limit, which is defined as that of the H_2/H_2O equilibrium condition, -3.34 eV [15]. We see that the average cost of an O vacancy increases linearly with the average energy per O atom for an M^{III}-O or M^{IV}-O bond (M^{III} and M^{IV} are the trivalent or 4-valent metals), although at a slower rate than 1:1. Of course, the overall O vacancy content also depends on the deposition conditions.

The second factor is the ON-current and the field-effect mobility. The density of states (DOS) in the band gap of a-IGZO is well known and is shown in Fig. 3(a) for reference [14]. It is notable that the DOS at the mobility edge at the top of the conduction band tail is ~10^{18} cm^{-3}, which is about 1000 times lower than the value for a-Si:H. Thus, the reduced disorder at the conduction band edge of a-IGZO is significant to allow its larger field-effect mobility.

The field-effect mobility can be expressed in terms of either the effective electron mass m*, or the degree of disorder of the conduction band edge states. Kumomi et al [19] have plotted the experimental field-effect mobilities of various amorphous binary In-metal oxides against the reciprocal of their effective mass of the single metal oxide. The oxide field-effect mobility was found to have an exponential dependence against the inverse effective mass of the single metal oxide in its crystalline state [19].

The degree of disorder at the conduction band edge also depends on the energy of the conduction band minimum of each component oxide, as shown in Fig. 3(b). This compares the band alignment among various possible n-type metal oxides referred to the vacuum level [38]. It is seen that Ga_2O_3 has a CB energy similar to that of ZnO or In_2O_3, as measured by photoemission spectroscopy [39], whereas that of other oxides like Al_2O_3, SiO_2, Y_2O_3 or HfO_2 of both main group metals or transition metals have a much higher CB energy referred to the vacuum level.

An important point is that despite the oxygen anion being common to these oxides, the oxygen non-bonding VBM state does not lie at a common energy in some systems [40]. This is due to the varying repulsive effect of filled cation d states on the valence band maximum [41]. Instead, the CB edge of Ga_2O_3 lies at similar energy to that in ZnO or In_2O_3 despite its band gap being 1.5 eV larger. Thus, if the host binary oxides consist of ZnO and In_2O_3, there is little disorder in the CBM energy if the third oxide added is Ga_2O_3. Ga_2O_3 will also have a larger O vacancy suppression effect than Zn or In in this three-component mix, from Fig. 2(a). The interesting case is that not only is the Ga_2O_3 CBM close to that of ZnO and In_2O_3, it is nearly the only suitable oxide in this respect. In contrast, most metal oxides with a greater ability to suppress the O vacancy like Al_2O_3, Y_2O_3, SiO_2, or HfO_2 (Fig. 2(a)) would all lead to a more pronounced CB disorder potential due to their much higher CB edge, Fig. 3(b). In other words, O vacancy suppression would only occur at a cost to mobility for the other alternatives like Al, Y, Hf, Ti, etc.

The degree of disorder is seen in more detail from the band structures of some spinel-structured oxide semiconductors, calculated with the HSE hybrid functional approximation, as shown in Fig. 4. We see that c-IGZO has a parabolic effective mass minimum, Fig. 4(a). However, for c-$In_2Hf_2ZnO_8$, we see that narrowly spaced Hf 5d conduction states lie not so far above the CBM, Fig. 4(d). This would reduce the band mobility value. The case of c-$In_2Ti_2ZnO_8$ is even more unusual, Fig. 4(e). Although Ti-O bonds have a large bond energy to cause a higher cost O vacancy, the Ti 3d states would lie close to the CBM and so if their states mix into the free-electron In CB states, they would reduce the mobility more than in the case of c-$In_2Hf_2ZnO_8$. Thus Ti is also a poor choice for third metal oxide.

We also consider the case of SiO_2 as the third oxide [23]. There have been already some experimental studies on ISZO TFTs, but the field-effect mobility for In-Si-O is lightly suppressed [23]. Si has the same valence as HfO_2. It is shown in a spinel lattice where it also has a CBM well above that of the host oxide, Fig. 4(f) and Fig. 5(f). As expected from of Fig. 3(b), SiO_2 has a much higher CBM state than ZnO etc., indicating a severe disorder of the conduction band edge state, which in turn leads to the field-effect mobility loss. This agrees with the experiments.

Figure 5 show the PDOS of final a-IGXO networks by the HSE functional. A similar degree of disorder results can be observed for a-ITZO in Fig. 5(e), where the Ti-d PDOS peak position in the conduction band lies much closer to the CBM, so it reduces the mobility more severely than in other oxides. On the other hand, the PDOS of other amorphous oxides does not show much apparent features.

A final question concerns the light-induced stability process or negative bias illumination stress instability (NBIS) [8-15,42,43]. This can be considered to be a persistent photoconductivity that occurs due to the excitation of electrons by 2.0 - 2.8 eV photons from filled traps lying just above the valence band edge, as seen by hard X-ray photoemission [8]. The NBIS can be a serious device problem for display applications. Its mechanism has been long discussed, and it has only recently been shown that it is related to the behaviour of hydrogen, following the infra-red characterisation of the oxides by Bang et al [42], and the mechanism of Li et al [15,43].

The top of the bulk VBM of IXZO oxide is due to O pπ states. Above this appear filled Zn-H-Zn 3-center bond states due to pairs of hydrogens bonded the Zn dangling bonds of the O vacancies [43]. These states occur in the band gap for metal oxides when the metal is Zn, In, Ga, Hf, La. Other metal–H–Zn combinations are possible as noted by Bang [42]. Reducing the hydrogen content of these films using industrial pumping systems is ongoing.

It is possible that Si alloying can contribute to this process because it forms less well mixed oxide networks with ZnO. The small solubility of SiO_2 in ZnO was found by Nakamura et al [44] with exceptional properties such as low work function and relatively higher mobility. Thus, the locally ZnO-rich and SiO_2-rich regions have different local VBM energies. Figure 6(a) shows an ideal ZnO:SiO_2 network with only Zn-O bonds or Si-O bonds. As shown in Fig. 6(b), the VBM of O atoms that only bonding to Si is deeper than other oxygens only bonding to Zn. Hydrogen has a greater affinity to bond to the SiO_2 rich region on the alloy, than the ZnO-rich regions, Fig. 6(c). In the SiO_2-rich region, H is unable to form states above the overall VBM of the alloy. It forms Si-O-H units with states only within the main valence band. Thus, its states do not lie above the overall VBM, where they can be excited by 2.8 eV photons. In this way SiO_2 could inhibit the photo-induced instability. H prefers not to form 3-center bonds but OH groups, if there are sufficient Si-O groups available. Then, no Si-H states lie above the VBM, as shown in Fig. 6(d), and so no NBIS excitation will occur.

Finally, WO_3 and MoO_3 have a very deep ionisation potential and a moderate gap [45,46]. It will also give any H induced state lying below the overall VBM. Thus, W will reduce any

photo-induced instability, as noted by Aikawa et al [23]. This deserves further experimental investigation. However, the deep CBM of the alloy due to the low lying CBM of WO_3 or MoO_3 lowers the overall mobility, so perhaps it is not the most effective method. On the other hand, SiO_2 has too high a CBM.

IV. Conclusions

In conclusion, our calculations find that among multiple candidates for the third oxide in IXZO (X=Ga, Al, Y, Hf, Ti, Si) oxides, Ga adequately suppresses the formation of oxygen vacancies, while not contributing to the disorder of the conduction band edge and the reduction of electron mobility, compared with more electropositive metals like Hf, Y or Al. These mechanisms consistently explain the observed behavior of three-component metal oxides of In-Ga-Zn-O as good amorphous semiconductors for display applications.

Acknowledgments: The authors acknowledge funding from EPSRC grant EP/P005152/1. We also thank the support from Supercomputing Wales under the project SCW1070.

Data Availability Statement: The data that support the findings of this study are available from the corresponding author upon reasonable request.

References

1. H. Hosono, M. Yasukawa, H. Kawazoe, J. Non-Cryst. Solids **203**, 334 (1996)
2. K. Nomura, H. Ohta, A. Takagi, T. Kamiya, H. Hosono, Nature **432**, 488 (2004)
3. H. Hosono, J. Non-Cryst. Solids **352**, 851 (2006)
4. J. Robertson, Phys. Stat. Solidi b **245**, 1026 (2008)
5. A. Walsh, J. L. F. DaSilva, S. H. Wei, Chem. Mater. **21**, 5119 (2009)
6. K. Nomura, T. Kamiya, H. Ohta, H. Hosono, Phys. Rev. B **75**, 035212 (2007)
7. T. Kamiya, H. Hosono, Sci. Tech. Adv. Mater. **11**, 044305 (2010); T. Kamiya, K. Nomura, H. Hosono, Phys. Stat. Solidi A **207**, 1698 (2010)
8. K. Nomura, T. Kamiya, H. Yanagi, E. Ikenaga, K. Yang, K. Kobayashi, M. Hirano, H. Hosono, Appl. Phys. Lett. **92**, 202117 (2008)
9. K. Ghaffarzadeh, A. Nathan, J. Robertson, S. Kim, S. Jeon, C. Kim, U. I. Chung, J. H. Lee, Appl. Phys. Lett. **97**, 113504 (2010)
10. B. Ryu, H. K. Noh, E. A. Choi, K. J. Chang, Appl. Phys. Lett. **97**, 022108 (2010)
11. H. K. Noh, K. J. Chang, B. Ryu, W. J. Lee, Phys. Rev. B, **84**, 115205 (2011)
12. P. Goerrn, M. Lehnhardt, T. Riedl, W. Kowalsky, Appl. Phys. Lett. **91**, 193504 (2009)
13. P. Migliorato, M. Chowdhury, J. G. Um, M. Seok, J. Jang, Appl. Phys. Lett. **101**, 123502 (2012)
14. J. Robertson, J. Non-Cryst. Solids **358**, 2437 (2012)
15. H. Li, Y. Guo, J. Robertson, Phys. Rev. Mater **2**, 074601 (2018)
16. C. J. Kim, S. Kim, J. H. Lee, J. S. Park, S. Kim, J. Park, E. Lee, J. Lee, Y. Park, J. H. Kim, S. T. Shin, U. I. Chung, Appl. Phys. Lett. **95**, 252103 (2009)
17. E. Chong, K. C. Jo, S. Y. Lee, Appl. Phys. Lett. **96**, 152102 (2009)
18. D. H. Cho, S. Yang, C. Byun, J. Shin, H. Y. Chun, Appl. Phys. Lett. **93**, 142111 (2008)
19. H. Kumomi, et al, J. Display Technol. **5**, 531 (2009)
20. H. W. Park, B. K. Kim, J. S. Park, K. B. Chung, Appl. Phys. Lett. **102**, 102102 (2013)
21. S. Parthiban, J. Y. Kwon, J. Mater. Res. **29**, 1585 (2014)
22. J. S. Park, W. J. Maeng, H. S. Kim, J. S. Park, Thin Solid Films **520**, 1679 (2012)
23. S. Aikawa, T. Nabatame, K. Tsukagoshi, Appl. Phys. Lett. **103**, 172105 (2013)
24. N. Saito, T. Sawabe, J. Kataoka, T. Ueda, T. Tezuka, K. Ikeda, Jpn. J. Appl. Phys. **58** SBBJ07 (2019)
25. N. Saito, K. Miura, T. Ueda, T. Tezuka, K. Ikeda, 2017 IEEE Electron Devices Technology and Manufacturing Conference (EDTM) 7A-4
26. N. Saito T. Udea, T. Tezuka, K. Ideka, IEEE J. Electron Devcies Soc. **6** 1253 (2018);
27. H. Ye, J. Gomez, W. Chakraborty, S. D. Spetalnick, S. Dutta, K. Ni, A. Raychowdhury,S. Datta, Tech Digest IEDM (2020)28.3
28. S. J. Clark, M. D. Segall, C. J. Pickard, P. J. Hasnip, M. J. Probert, K. Refson, and M. C. Payne, Z. Kristallogr. **220**, 567 (2005)
29. A. M. Rappe, K. M. Rabe, E. Kaxiras, and J. D. Joannopoulos, Phys. Rev B **41**, 1227 (1990)
30. A Janotti, D. Segev, and C. G. van der Walle, Phys. Rev. B **74**, 045202 (2006)
31. S. Lany and A. Zunger, Phys. Rev. Lett. **98**, 045501 (2007)
32. V. V. Anisimov, J. Zaanen, and O. K. Andersen, Phys. Rev. B 44, 943 (1991)
33. Z. Zhang, Y. Guo, and J. Robertson, Phys. Rev. Materials **4**, 054603 (2020)
34. J. Heyd, G. E. Scuseria, and M. Ernzerhof, J. Chem. Phys. **118**, 8207 (2003)
35. F. Oba, A. Togo, I. Tanaka, J. Paier, and G. Kresse, Phys. Rev. B **77**, 245202 (2008)
36. J. Robertson, O. Sharia, A. A. Demkov, Appl. Phys. Lett. **91**, 132912 (2007)
37. H. B. Michaelson, J. Appl. Phys. **48**, 4729 (1977)
38. J. Robertson, J. Vac. Sci. Technol. A **31** (5), 050821 (2013)
39. J. Kim, J. Bang, N. Nakamura, H. Hosono, APL Materals **7** 022501 (2018)

40. A. Klein, J. Am. Ceram. Soc. **96**, 331 (2013).
41. S. H. Wei, A. Zunger, Phys. Rev. Lett. **59**, 144 (1987)
42. J. Bang, S. Matsuishi, H. Hosono, Appl. Phys. Lett. **110**, 232105 (2017)
43. H. Li, Y. Guo, J. Robertson, Sci. Rep. **7**, 16858 (2017)
44. N. Nakamura, J. Kim, and H. Hosono, Adv. Electron. Mater. **4**, 1700352 (2018)
45. M. T. Greiner, M. G. Helander, W. M. Tang, W. B. Wang, J. Qiu, Z. H. Lu, Nature Mat. **11**, 76 (2012)
46. Y. Guo, J. Robertson, Appl. Phys. Lett. **105**, 222110 (2014)

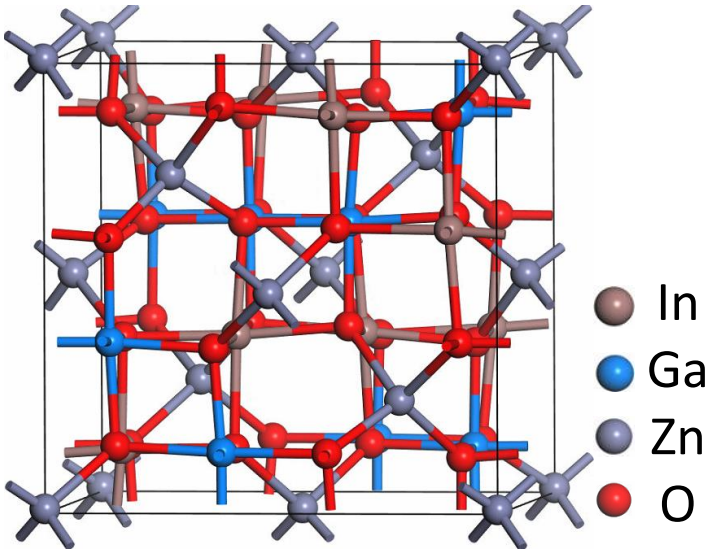

Fig. 1 Structure of spinel-type c-IGZO.

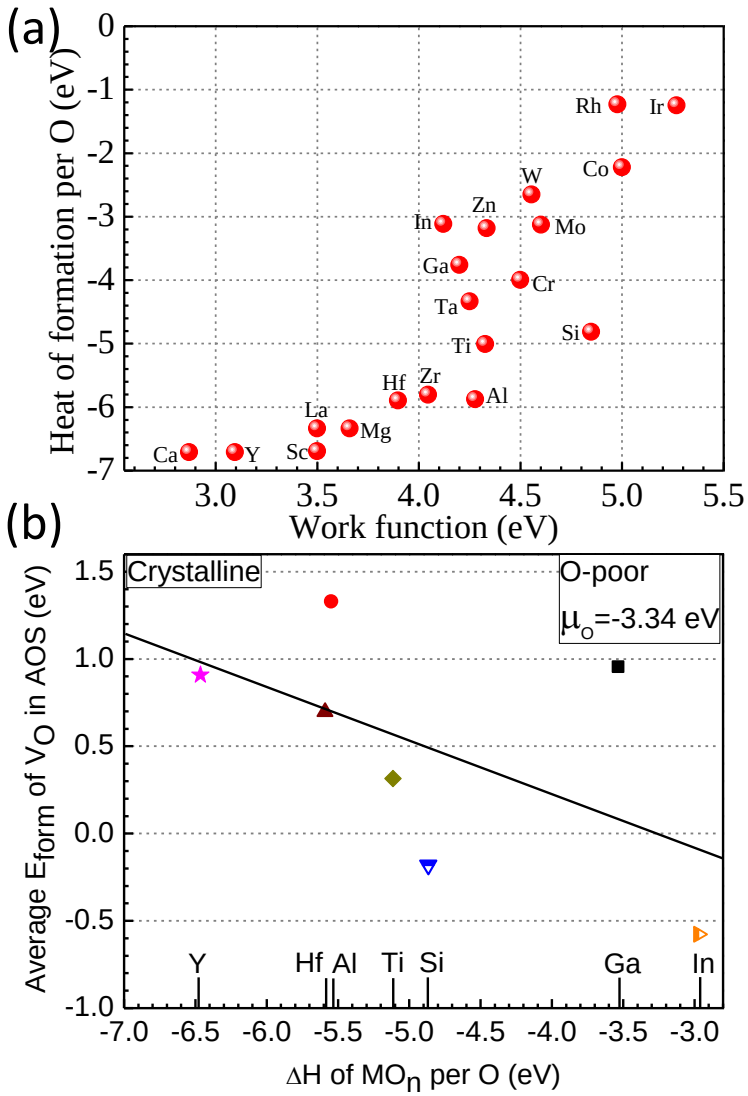

Fig. 2(a). Experimental heat of formation of bulk metal oxide per O atom versus metal work function. (b) Weighted average formation energies of Vo in crystalline-amorphous oxide semiconductors, versus calculated heat of formation of bulk metal oxide, with the Vo site number as the weight.

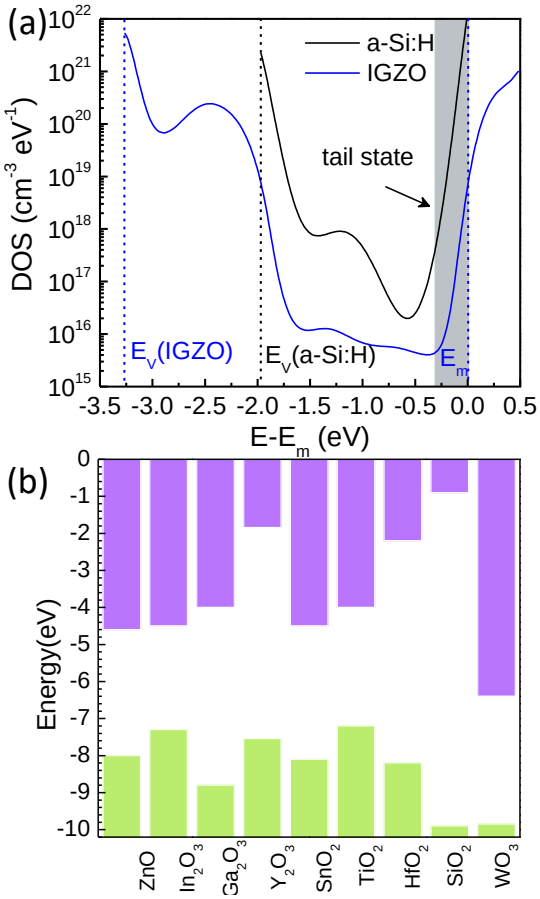

Fig. 3. (a) Schematic gap DOS comparison between IGZO and a-Si:H. (b) Band alignment of various n-type oxides, referred to the vacuum level.

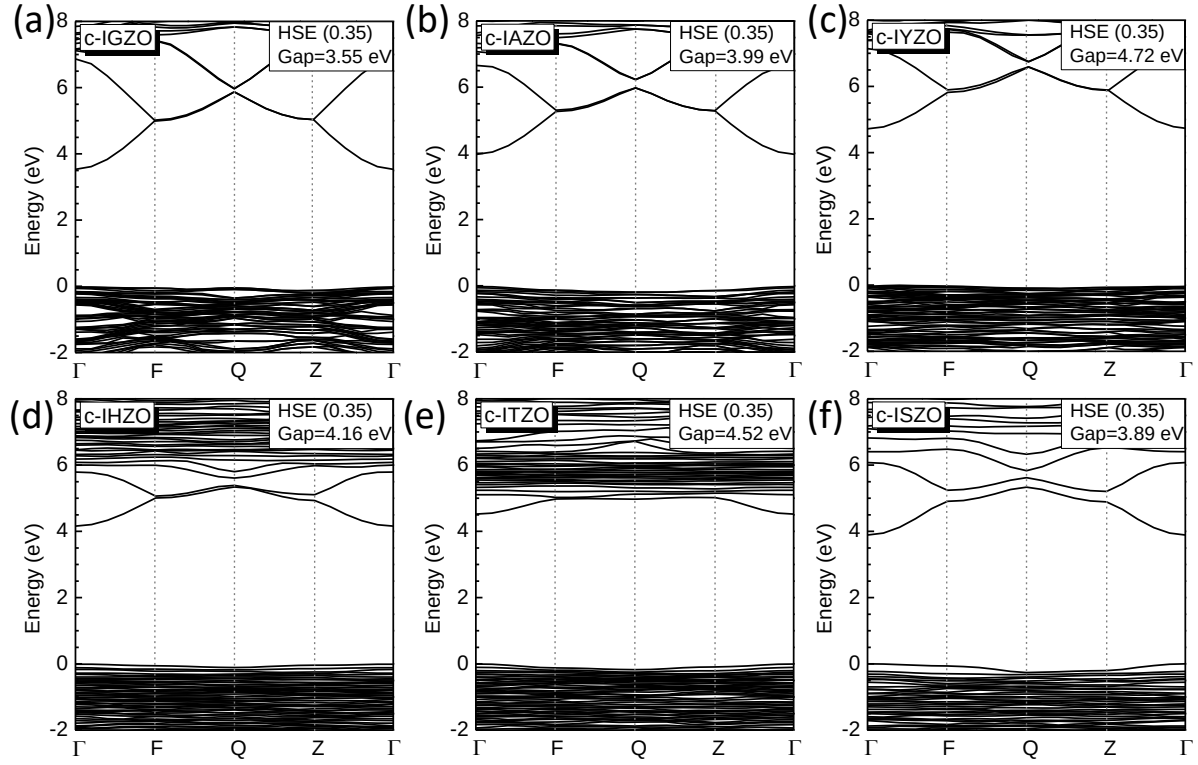

Fig. 4 Band structures of spinel-type (a) c-InGaZnO, (b) c-InAlZnO, (c) c-InYZnO, (d) c-InHfZnO, (e) c-InTiZnO, and (f) c-InSiZnO structures by HSE functional. The Hf-d and Ti-d states are labelled by blue arrows.

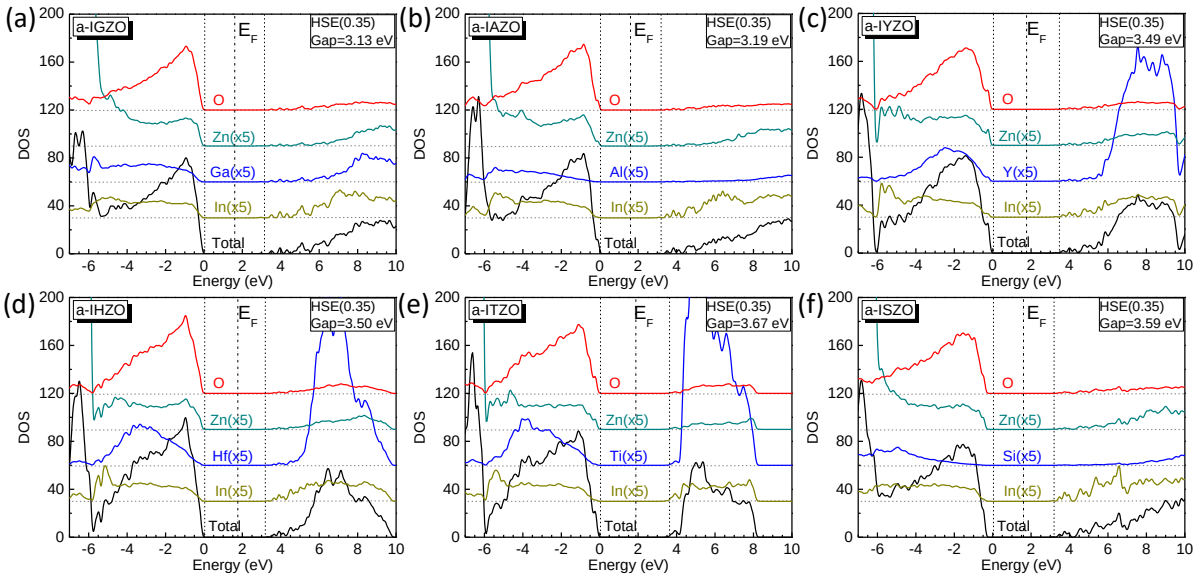

Fig. 5. PDOS of (a) a-InGaZnO, (b) a-InAlZnO, (c) a-InYZnO, (d) a-InHfZnO, (e) a-InTiZnO, and (f) a-InSiZnO networks by HSE functional. The VBM is referred to 0 eV. No gap states emerge and Fermi level lies at midgap. Vertical dashed lines indicate Ev and Ec.

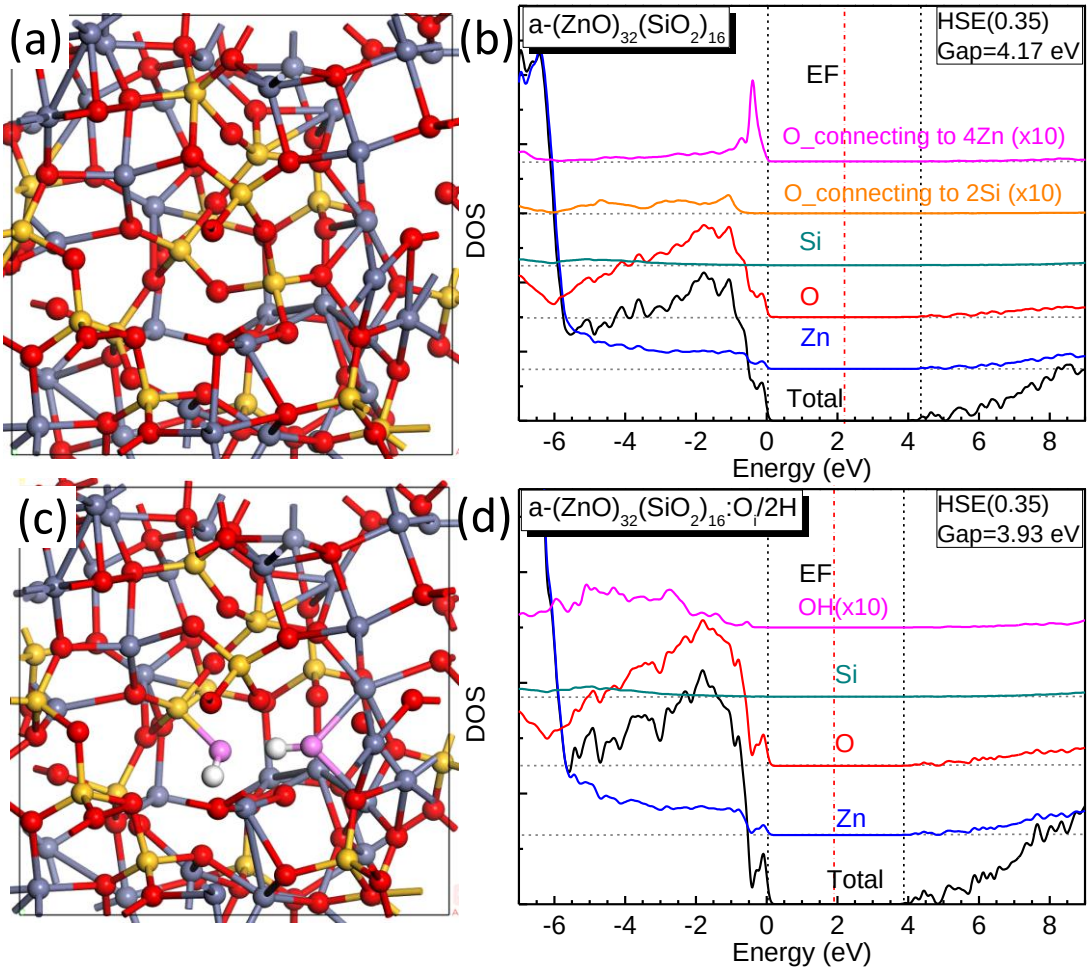

Fig. 6. Structure and PDOS of a-ZnO:SiO_2 network. (a) and (b) ideal a-ZnO:SiO_2. (c) a-ZnO:SiO_2 with an interstitual O, initially forming the Si-O-O-Si bridge, but the bridge breaks once the H is induced, forming two OH group. The grey, yellow, white, red and pink spheres are Zn, Si, H, O, and O of OH group, respectively. Vertical dashed lines indicate Ev and Ec.

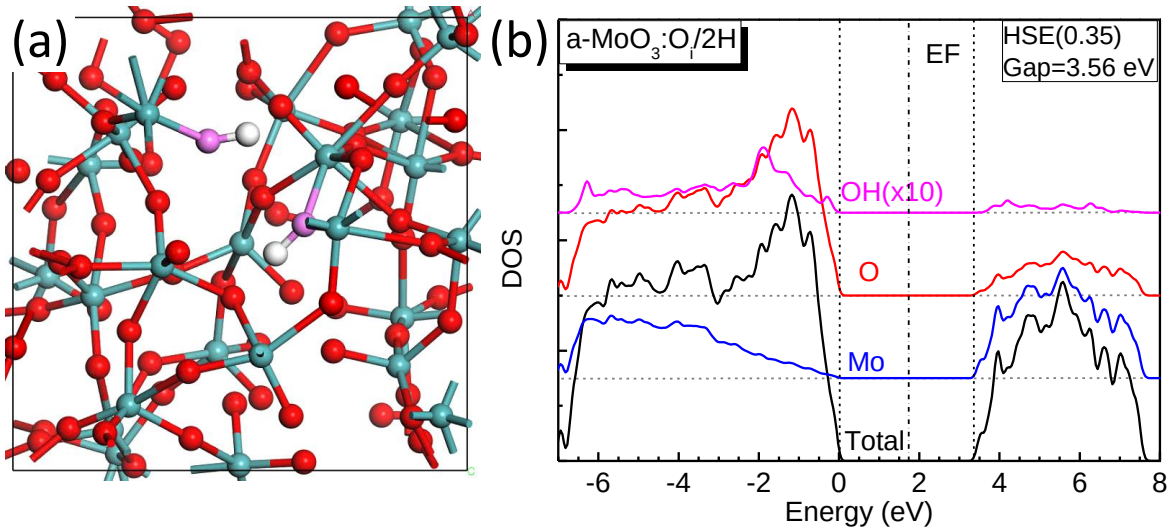

Fig. 7. (a) Structure and (b) PDOS of a-MoO_3 network with an interstitual O and two H. The initial -O-O- bridge breaks once the H is induced, forming two OH group.